SCIENCE CHINA
Chemistry

• ARTICLES •

February 2017 Vol.60 No.2: 237–242
doi: 10.1007/s11426-016-0369-y

Synthesis of poly(pyridine-imide)s and their electronic memory performances

Haifeng Chen, Linxin Wu, Xiong Xiao, Hongliang Wang, Jun Jiang, Lihua Wang, Qingfeng Xu* & Jianmei Lu*

College of Chemistry, Chemical Engineering and Materials Science, Collaborative Innovation Center of Suzhou Nano Science and Technology, Soochow University, Suzhou 215123, China

Received September 7, 2016; accepted November 13, 2016; published online January 3, 2017

In this paper, poly(pyridine-imide)s, PI-Ph and PI-Naphth, were successfully synthesised and fabricated for use as memory devices. The Al/PI-Ph/indium tin oxide (ITO) device showed dynamic random access memory characteristics, whereas Al/PI-Naphth/ITO showed rewritable (FLASH) memory characteristics. Characterisation of their UV, cyclic voltammograms, and density functional theory, were used to illustrate the different memory behaviours. The results show that the stability of electric-field-induced-charge-transfer complexes can affect memory performance.

poly(pyridine-imide)s, memory device, charge-transfer

Citation: Chen H, Wu L, Xiao X, Wang H, Jiang J, Wang L, Xu Q, Lu J. Synthesis of poly(pyridine-imide)s and their electronic memory performances. *Sci China Chem*, 2017, 60: 237–242, doi: 10.1007/s11426-016-0369-y

1 Introduction

In recent decades, the storage capacity of the conventional Si-based materials has approached physical limits according to Moore's law. As one of the potential "next generation memories", polymeric material-based memory devices have attracted considerable attention because of their low-cost potential, flexibility, high-density data storage, and miniaturisation [1–7]. However, their molecular structures exert significant influences on their memory performance [8]. For example, polyimides have been selected as promising information-storage materials due to their high thermal stability, superior mechanical properties, low dielectric constants, and the high controllability of their structures [9–16]. By optimising the side chain structure of many polyimides, many possible memory effects can be obtained, including the volatile memory effects of dynamic random access memory (DRAM) [12] and static random access memory (SRAM) [17], or the non-volatile memory effects of write-once read-many times (WORM) [14] memory and rewritable (FLASH) [9] memory. However, most of the studies were focused on edge modification, and the biphenyl backbone is seldom substituted. Compared with benzene, pyridine is an electron-deficient aromatic heterocycle and has improved electron-transport properties [18,19], so pyridine was chosen as part of the backbone of the polymers discussed herein instead of benzene.

In this paper, poly(pyridine-imide)s: PI-Ph (2-(4-(4-(9-ethyl-9*H*-carbazol-3-yl)-6-(p-tolyl) pyridin-2-yl)phenyl)-6-methylpyrrolo[3,4-f]isoindole-1,3,5,7(2*H*,6*H*)-tetraone) and PI-Naphth (2-(4-(4-(9-ethyl-9*H*-carbazol-3-yl)-6-(*p*-tolyl)-pyridin-2-yl)phenyl)-7-methylbenzo[lmn][3,8]phenanthroline-1,3,6,8(2*H*,7*H*)-tetraone, Scheme 1) were successfully synthesised. PI-Ph was synthesised by polycondensation of monomer CBAPP with 1,2,4,5-benzenetetracarboxylic anhydride and the following chemical imidization of acetic

*Corresponding authors (email: xuqingfeng@suda.edu.cn; lujm@suda.edu.cn)

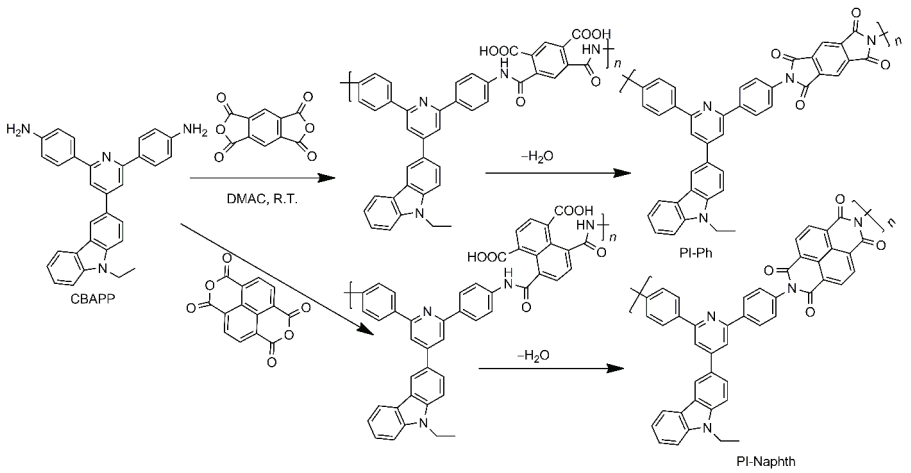

Scheme 1 The synthesis and chemical structures of poly(pyridine-imide)s (PI-Ph and PI-Naphth).

anhydride and pyridine. The synthetic process used for PI-Naphth was similar to that used for PI-Ph. Both PI-Ph and PI-Naphth were prepared and used as active layers in a sandwiched memory device (Figure 1). PI-Ph, and PI-Naphth-based devices show different electrical switching effects. PI-Ph-based devices exhibited non-volatile WORM type memory performance. While PI-Naphth-based devices exhibited non-volatile FLASH type memory performance. Due to the distinct degrees of π-π* conjugation, PI-Ph and PI-Naphth can form various charge transfer complexes [8]. Characterisation of UV, cyclic voltammograms, and density functional theory were used to illustrate these different memory behaviours. The results show that the stability of electric-field-induced-charge-transfer complexes can affect the memory performances thereof.

2 Experimental

2.1 Materials

4-Nitroacetophenone, *N*-ethyl-3-carbazolecarboxaldehyde, and 1,4,5,8-naphthalenetetracarboxylic dianhydride were ordered from Tokyo Chemical Industry (TCI, Japan). Acetic anhydride, 1,2,4,5-benzenetetracarboxylic anhydride, palladium on activated carbon (10% Pd), ammonium acetate, glacial acetic acid, ethanol, methyl alcohol, *N*,*N*-dimethylformamide (DMF), hydrazine hydrate, propylene oxide, azabenzene, 1-methyl-2-pyrrolidinone (NMP), and *N*,*N*-dimethylacetamide (DMAc) were purchased from Sinopharm Chemical Reagent Co. Ltd (China). Azabenzene was purified by distillation. All other reagents and solvents were used as received without further purification. 3-(2,6-bis(4-Nitrophenyl)pyridin-4-yl)-9-ethyl-9*H*-carbazole (CBNPP) and 4,4′-(4-(9-ethyl-9*H*-carbazol-3-yl)pyridine-2,6-diyl) dianiline (CBAPP) were synthesised according to the methods

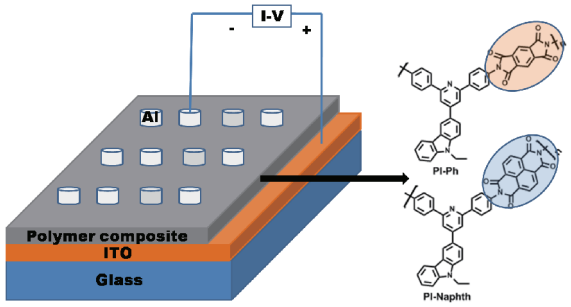

Figure 1 A sandwiched memory device (color online).

described in the literature [18].

2.2 Molecular synthesis

2.2.1 3-(2,6-Bis(4-nitrophenyl)pyridin-4-yl)-9-ethyl-9*H*-carbazole (CBNPP)

A solution of 4-nitroacetophenone (40 mmol, 6.61 g), *N*-ethyl-3-carbazolecarboxaldehyde (20 mmol, 4.47 g), ammonium acetate (0.4 mol, 30.83 g), and glacial acetic acid (96 mL) was stirred for 1 h at 90 °C in a 150 mL round-bottomed flask. Then the mixture was stirred under reflux for 3 d. After cooling, the solution was filtered and the obtained crude product was recrystallised from *N*,*N*-dimethylacetamide to give a yellow powder (mass, 4.64 g), equating to a yield of 45%. ^{1}H NMR data included: (400 MHz, DMSO-d_6) δ 8.97 (s, 1H), 8.65 (d, J=8.3 Hz, 4H), 8.57 (s, 2H), 8.38 (d, J=8.3 Hz, 4H), 8.32 (d, J=7.7 Hz, 1H), 8.23 (d, J=8.3 Hz, 1H), 7.77 (d, J=8.4 Hz, 1H), 7.66 (d, J=8.2 Hz, 1H), 7.51 (t, J=7.6 Hz, 1H), 7.28 (t, J=7.4 Hz, 1H), 4.51 (q, J=6.9 Hz, 2H), 1.35 (t, J=7.1 Hz, 3H) (Figure S1, Supporting Information online).

2.2.2 4,4′-(4-(9-Ethyl-9*H*-carbazol-3-yl)pyridine-2,6-diyl) dianiline (CBAPP)

A solution of CBNPP (8.6 mmol, 4.43 g), 10 % Pd/C (0.15 g)

and ethanol (35 mL) was heated at 90 °C while being stirred. Hydrazine hydrate (20 mL) was slowly added to the mixture. The final mixture was stirred for 24 h. The solution was hot-filtered to remove the Pd/C. The filtrate was cooled, filtered, and the obtained crude product was recrystallised from ethanol to give a white powder (mass, 1.96 g), equating to a yield of 50%. ^{1}H NMR data included: (400 MHz, DMSO-d_6) δ 8.85 (s, 1H), 8.38 (d, J=7.7Hz, 1H), 8.08 (d, J=8.5Hz, 5H), 7.96 (s, 2H), 7.75 (d, J=8.6Hz, 1H), 7.66 (d, J=8.2Hz, 1H), 7.51 (t, J=7.6Hz, 1H), 7.27 (t, J=7.4Hz, 1H), 6.72 (d, J=8.5 Hz, 4H), 5.43 (s, 4H), 4.51 (q, J=6.9Hz, 2H), 1.36 (t, J=7.1 Hz, 3H) (Figure S2).

2.2.3 2-(4-(4-(9-Ethyl-9*H*-carbazol-3-yl)-6-(*p*-tolyl)-pyridin-2-yl)phenyl)-6-methylpyrrolo[3,4-f]isoindole-1,3,5,7 (2*H*,6*H*)-tetraone (PI-Ph)

CBAPP (2 mmol) was added to the DMAc (10 mL) and stirred vigorously at 0 °C under a nitrogen atmosphere. 1,2,4,5-Benzenetetracarboxylic anhydride (2 mmol) was added to the mixture. After 1 h, the ice-water bath was removed and the reaction was allowed to continue for 24 h at room temperature. The solution was filtered and poured into a large amount of water. The precipitated product was washed by water and methyl alcohol to give poly(amic acid). Acetic anhydride (10 mL) and azabenzene (5 mL) were added to the solution of poly(amic acid) (1 g) in NMP, the mixture was stirred at 110 °C under a nitrogen atmosphere for 6 h. The polymer solution was poured into methanol. The precipitate was filtered, and the obtained crude product was washed by methanol to give an orange powder. The orange powder was dried in a vacuum oven, overnight, at 120 °C to give a mass of 0.6 g, equating to a yield of 72%.

2.2.4 2-(4-(4-(9-Ethyl-9*H*-carbazol-3-yl)-6-(*p*-tolyl)-pyridin-2-yl)phenyl)-7-methylbenzo[lmn][3,8]phenanthroline-1,3,6,8(2*H*,7*H*)-tetraone (PI-Naphth)

The synthesis of PI-Naphth used a similar method to that used for PI-Ph. The difference is that 1,2,4,5-benzenetetracarboxylic anhydride is replaced by 1,4,5,8-naphthalenetetracarboxylic dianhydride to give a final yield of 68%.

2.3 Measurements

All of the electrical measurements were characterised at room temperature. ^{1}H NMR spectra were evaluated on a Varian INOVA 400 MHz FT-NMR Spectrometer (USA). The number average (M_n), weight-average (M_w) molecular weight, and polydispersity index (PDI) were recorded by gel-permeation chromatography (GPC) on a Waters1515 Gel Chromatograph (USA) with *N*,*N*-dimethylformamide (DMF) as an eluent. Thermogravimetric analysis (TGA) was undertaken on a TA Instruments Dynamic TGA 2950 (USA) at a heating rate of 20 °C min^{-1} under an N_2 flow rate of 20 mL min^{-1}. UV-visible (UV-Vis) absorption spectra were determined by a Perkin-Elmer-l-17 spectrophotometer (USA) under ambient conditions. Cyclic voltammetry (CV) measurements were performed at room temperature using an ITO working electrode, a reference electrode (Ag/AgCl), and a counter electrode (Pt wire) at a sweep rate of 20 mV s^{-1} (CorrTest CS Electrochemical Workstation Analyzer, USA) in a 0.1 M acetonitrile solution of tetrabutylammonium hexafluorophosphate (n-Bu_4NPF_6). Atomic force microscopy (AFM) measurements were carried out by using an MFP-3DTM (Digital Instruments/Asylum Research) AFM instrument (UK). Fourier transform infrared (FT-IR) spectra of the poly(pyridine-imide)s were recorded on a Varian CP-3800 spectrometer (USA) in the range of 4000–400 cm^{-1}.

2.4 Fabrication of the memory device

The indium tin oxide (ITO) glass substrate was cleaned sequentially with deionised water, acetone, and alcohol for 30 min using an ultrasonic bath. PI-Ph and PI-Naphth at a concentration of 10 mg mL^{-1} were prepared in the DMF to form solutions thereof. The solutions were filtered through micro-filters with a pinhole size of 0.45 mm, then spin-coated onto a clean ITO glass substrate at a speed of 2000 r min^{-1} for 30 s. The resulting film was annealed in a vacuum chamber at 10^{-1} Pa and 80 °C for 10 h. The top metal electrode was a 150 nm-thick sheet with a radius of 0.2 mm of Al, which was thermally evaporated at about 10^{-6} torr through a shadow mask. Two devices ITO (70 nm)/PI-Ph (70 nm)/Al (150 nm) and ITO (70 nm)/PI-Naphth (70 nm)/Al (150 nm) were fabricated (Figure S3) and they had been optimized according to the previous work of our group. The active area of the fabricated device was 0.126 mm^2 (in the form of a nummular point with a radius of 0.2 mm).

3 Results and discussion

3.1 Synthetic routes

Scheme 1 shows the synthetic routes of poly(pyridine-imide)s (PI-Ph and PI-Naphth): a more detailed synthetic procedure is given in the experimental section. Scheme S1 (Supporting Information online) shows the synthetic routes of CBNPP and CBAPP.

3.2 Polymer characterisation and thermal stabilities

The poly(pyridine-imide)s were successfully synthesised by polycondensation. The structures of poly(pyridine-imide)s were characterised by ^{1}H NMR (Figure S4). The characteristic signals at 5.43 ppm assigned to the amino moieties in monomer could not be observed in the pattern of the polymer. The characteristic absorptions of poly(pyridine-imide)s in FT-IR spectrum from the amino groups were absent, and

new absorptions from the imide moieties at 1790 cm^{-1} (ν_{as}, C=O),1720 cm^{-1} (ν_s, C=O),and 1390 cm^{-1} (ν, C−N) appeared (Figure S5). Both ^{1}H NMR and FT-IR indicated the successful synthesis of poly(pyridine-imide)s. GPC showed that the number-average molecular weights of PI-Ph and PI-Naphth were about 5440 with a polydispersity index (PDI) of 1.01 and 5400 with PDI of 1.03 respectively. The 5% weight-loss temperatures ($T_{d\,5\%}$) of PI-Ph and PI-Naphth were found to be 312 and 324 °C, respectively (Figure S6). The good thermal stability of the poly(pyridine-imide)s is essential for their application as active materials in electronic devices [7].

3.3 Optical characterisation

The UV-Vis spectra of PI-Ph and PI-Naphth in dilute solution and thin film are shown in Figure 2. The maximum absorption peak of PI-Ph and PI-Naphth in DMF solution were at 302 and 303 nm and originated from the π-π* transition of the carbazole ring, respectively. The longer peak at 340 and 345 nm was attributed to charge transfer in the carbazole group and imide ring [20,21]. Compared with the absorption band in solution, the band of PI-Ph and PI-Naphth in their thin film states underwent a slight red-shift and was slightly broadened due to the formation of molecular aggregations.

3.4 Film morphology

Figure 3 shows AFM images of thin, spin-coated, poly(pyridine-imide)s films which had relatively smooth, continuous surfaces. The root-mean-square roughness of the PI-Ph and PI-Naphth films was 3.18 and 1.30 nm, respectively. The lower roughness values indicated that the films were suitable for use in electronic devices.

3.5 Electrochemical properties

The electrochemical properties of PI-Ph and PI-Naphth films were investigated by using conducting cyclic voltammetry (Figure S7). The optoelectronic properties and calculated energy levels of poly(pyridine-imide)s are summarised in Table 1. The highest occupied molecular orbital (HOMO) and lowest unoccupied molecular orbital (LUMO) energy levels could be calculated from the UV-Vis absorption spectra and the CV results by the following equations [22,23]:

$$E_{HOMO} = -(E_{OX} + 4.8 - E_{Foc}) \quad (1)$$

$$E_{LUMO} = E_{HOMO} + E_g \quad (2)$$

where E_{OX} is the onset oxidation potential, E_{Foc} is the external standard potential of the ferrocene/ferrocenium ion couple, and E_g is the band gap determined from the UV-Vis absorption spectra. The E_{Foc} was 0.43 eV from the CV measurement with a bare ITO glass substrate without any organic films thereon.

3.6 Electrical switching effects

The memory behaviour of the devices was measured through their current-voltage (*I-V*) characteristics. Al and ITO were used as the cathode and anode respectively in all memory devices. The current-voltage characteristic of the ITO/PI-Ph/Al device is shown in Figure 4(a). The device remained in a high-resistance (OFF) state when a negative voltage was applied from 0 to –2.4 V. A sharp transition in the current was observed from the OFF state to the low-resistance (ON) state at the switching threshold voltage (V_{th}) of approximately –2.4

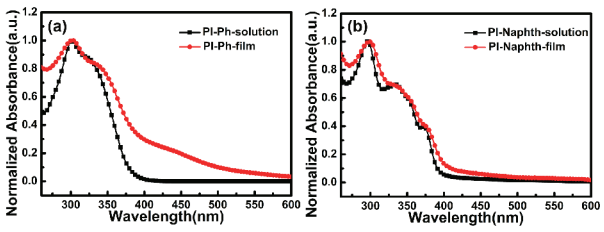

Figure 2 UV-Vis absorption spectra of (a) PI-Ph, (b) PI-Naphth in DMF solution and in the thin film state on a quartz plate (color online).

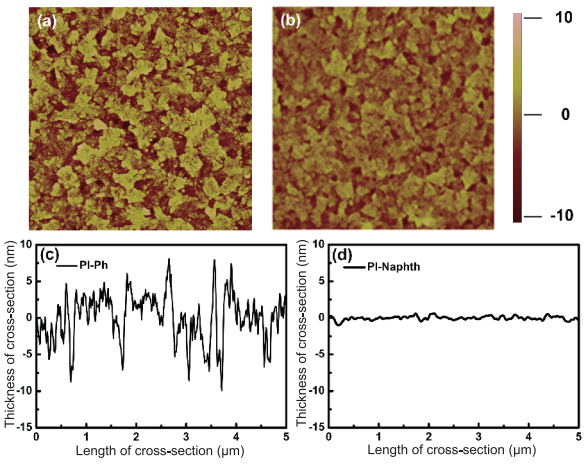

Figure 3 (a, b) Tapping-mode (5 μm×5 μm) AFM topography; (c, d) typical cross-section profile of AFM topographic image of PI-Ph and PI-Naphth thin films spin-coated onto ITO substrates (color online).

Table 1 Optoelectronic properties and calculated energy levels of all compounds

Sample	λ_{onset} (nm) (film)	E_g [a)] (eV)	E_{ox} (V)	HOMO [b)] (eV)	LUMO (eV)
PI-Ph	390	3.18	1.35	–5.72	–2.54
PI-Naphth	410	3.02	1.06	–5.43	–2.41

a) The data was calculated by the following equation: bandgap=1240/λ_{onset} of films; b) the HOMO energy levels were calculated from cyclic voltammetry and were referenced to ferrocene (4.8 eV).

V. Such an OFF-to-ON transition could be regarded as the "writing" process. Additionally, the device could be kept in this ON state during sweeps 2 and 3 from 0 to –5 V or from 0 to 5 V (the "reading" process). The ITO/PI-Ph/Al device exhibited a typical non-volatile WORM memory characteristic with an ON/OFF ratio of 2.8×10^3.

The current-voltage characteristic of the ITO/PI-Naphth/Al device is shown in Figure 4(b). The device remained in an OFF state when a negative voltage was applied from 0 to –1.1 V. A sharp transition in current was observed from the OFF state to the ON state at the switching threshold voltage of approximately –1.1 V. The device could be kept in this ON state when the subsequent second sweep was applied from 0 to –5 V. However, the device could return to the original OFF state at the switching threshold voltage of approximately 3.1 V, when sweep 3 m from 0 to 5 V, was applied. Such an ON-to-OFF transition could be regarded as the "erasing" process. The device remained in the OFF state when sweep 4 was applied from 0 to 5 V. The OFF state could be switched to an ON state once again when sweep 5 was applied from 0 to –5 V, which indicated that the device was rewritable and erasable. Therefore, the memory device exhibited a non-volatile flash memory characteristic with an ON/OFF ratio of 7.1×10^3.

The stability of the devices was evaluated through retention time testing by applying voltage from 0 to –5 V and 0 to 5 V alternately in 10000 s. No significant degradation was observed in the device in the low resistance state (LRS) and high resistance state (HRS) after 10000 s during the continuous stress test (Figure S8), indicating the stability of the active layer.

When the top electrode was substituted for gold, the memory devices also exhibited similar memory performances (Figure 4(c, d)) indicating that current changes were not caused by metal filament penetration [24,25].

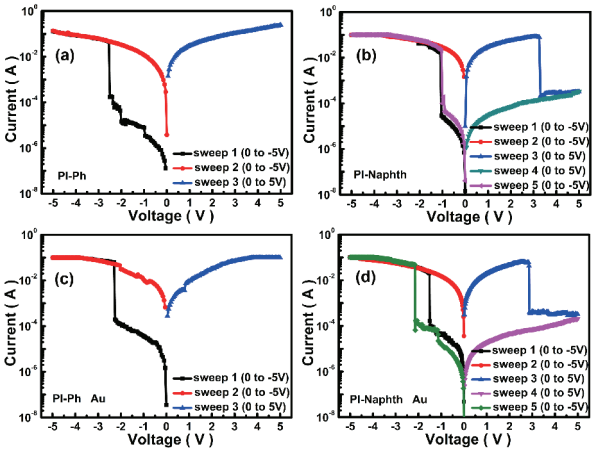

Figure 4 Current-voltage (*I-V*) characteristics of (a) PI-Ph and (b) PI-Naphth memory devices based on an ITO-Al electrode; *I-V* characteristics of (c) PI-Ph and (d) PI-Naphth memory devices based on an ITO-Au electrode (color online).

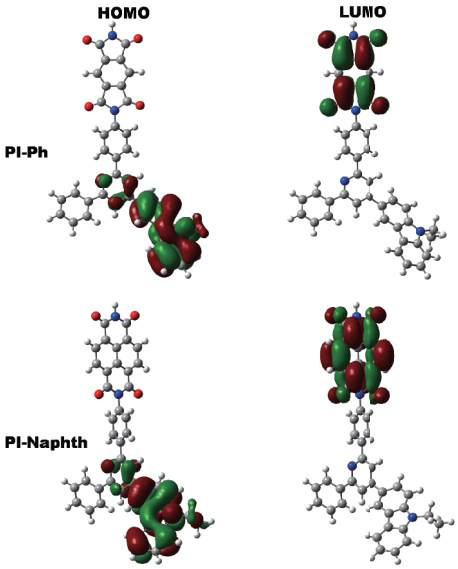

Figure 5 HOMO and LUMO surfaces of PI-Ph and PI-Naphth obtained by simulation based on B3LYP/6-31G(d) model chemistry (color online).

3.7 Proposed storage mechanism

The theoretical data for poly(pyridine-imide)s segments are shown in Figure 5, in which the HOMO orbital was mainly located at the π orbital and the electron cloud mainly distributed in the carbazole group, while the LUMO orbital was at the π* orbital and the electron cloud was mainly distributed in the imide ring [20]. We could speculate that a charge-transfer (CT) interaction could be formed, which gave a bistable electric performance [26]. Before reaching the threshold voltage, the charge carriers were difficult to transfer because of the obstacle formed by the pyridyl group and imide ring and the devices were thus in an OFF state. When the voltage was continuously increased, the electrons, located in the ground state, would reach a higher energy level by way of an external excitation transition and promote charge transfer from the carbazole group to the imide ring. This process was considered as a CT interaction [27]. Once the CT state was formed, a charge transport channel was also formed. Charge carriers could easily migrate through the open channel, the current increased sharply and the device reached the ON state. The stability of CT complexes formed by the carbazole group and two kinds of imide ring, determined the type of storage offered by each device [28]. Since PI-Ph and PI-Naphth had a great degree of π-π* conjugation, the resulting CT complex was relatively stable, and thus gave rise to a bistable electrical performance; however, the E_g (3.18 eV) of PI-Ph was larger than the E_g (3.02 eV) of PI-Naphth, which indicated that the CT complex of PI-Ph was more stable than that of PI-Naphth, so, when a negative voltage was applied, the current did not decrease, and the ITO/PI-Ph/Al device showed

non-volatile storage performance. Even when a positive voltage sweep was applied from 0 to 5 V, the CT complex of PI-Ph remained stable and showed WORM memory performance; however, the CT complex of PI-Naphth was dissociated when a positive voltage sweep was applied at about 3.1 V. The conductive paths disappeared, which led to current mutation. The ITO/PI-Ph/Al device was changed from the ON state to an OFF state. This was called an "erase" process and the PI-Naphth-based device showed a flash memory performance. However, compared with the "write" process, the "erase" process required more energy, so the "erase" voltage was higher than the threshold voltage required for the "write" process.

4 Conclusions

Poly(pyridine-imide)s, PI-Ph and PI-Naphth, were successfully synthesised. *I-V* measurements indicated that these poly(pyridine-imide)s exhibited different electrical switching phenomena. PI-Ph-based devices exhibited non-volatile WORM type memory performance. PI-Naphth-based devices exhibited non-volatile flash type memory performance. Due to the distinct degrees of π-π* conjugation, these poly(pyridine-imide)s could form different charge-transfer complexes, which could lead to different stable states of high conductivity. The result showed that the stability of electric-field-induced-charge-transfer complexes could affect their memory behaviour, which might generate useful ideas for the design of high-performance memory materials.

Acknowledgments This work was supported by the National Natural Science Foundation of China (21336005, 21371128), and the major research project of Jiangsu Province Office of Education (15KJA150008).

Conflict of interest The authors declare that they have no conflict of interest.

Supporting information The supporting information is available online at http://chem.scichina.com and http://link.springer.com/journal/11426. The supporting materials are published as submitted, without typesetting or editing. The responsibility for scientific accuracy and content remains entirely with the authors.

1 Ree BJ, Kwon W, Kim K, Ko YG, Kim YY, Lee H, Ree M. *ACS Appl Mater Interfaces*, 2014, 6: 21692–21701
2 Shi L, Tian G, Ye H, Qi S, Wu D. *Polymer*, 2014, 55: 1150–1159
3 Chen CJ, Yen HJ, Hu YC, Liou GS. *J Mater Chem C*, 2013, 1: 7623
4 Ko YG, Kim DM, Kim K, Jung S, Wi D, Michinobu T, Ree M. *ACS Appl Mater Interfaces*, 2014, 6: 8415–8425
5 Patil S, Datar S, Rekha N, Asha SK, Dharmadhikari CV. *Nanoscale*, 2013, 5: 4404–4411
6 Hwang SK, Choi JR, Bae I, Hwang I, Cho SM, Huh J, Park C. *Small*, 2013, 9: 831–837
7 Kurosawa T, Lai YC, Higashihara T, Ueda M, Liu CL, Chen WC. *Macromolecules*, 2012, 45: 4556–4563
8 Lin WP, Liu SJ, Gong T, Zhao Q, Huang W. *Adv Mater*, 2014, 26: 570–606
9 Liu YL, Ling QD, Kang ET, Neoh KG, Liaw DJ, Wang KL, Liou WT, Zhu CX, Chan DSH. *J Appl Phys*, 2009, 105: 044501–044501
10 Kim K, Park S, Hahm SG, Lee TJ, Kim DM, Kim JC, Kwon W, Ko YG, Ree M. *J Phys Chem B*, 2009, 113: 9143–9150
11 Liu CL, Kurosawa T, Yu AD, Higashihara T, Ueda M, Chen WC. *J Phys Chem C*, 2011, 115: 5930–5939
12 Wang KL, Liu YL, Shih IH, Neoh KG, Kang ET. *J Polym Sci A-Polym Chem*, 2010, 48: 5790–5800
13 Kim DM, Park S, Lee TJ, Hahm SG, Kim K, Kim JC, Kwon W, Ree M. *Langmuir*, 2009, 25: 11713–11719
14 Wang KL, Liu YL, Lee JW, Neoh KG, Kang ET. *Macromolecules*, 2010, 43: 7159–7164
15 You NH, Chueh CC, Liu CL, Ueda M, Chen WC. *Macromolecules*, 2009, 42: 4456–4463
16 Lee TJ, Chang CW, Hahm SG, Kim K, Park S, Kim DM, Kim J, Kwon WS, Liou GS, Ree M. *Nanotechnology*, 2009, 20: 135204
17 Liu YL, Wang KL, Huang GS, Zhu CX, Tok ES, Neoh KG, Kang ET. *Chem Mater*, 2009, 21: 3391–3399
18 Huang YC, Wang KL, Lee WY, Liao YA, Liaw DJ, Lee KR, Lai JY. *J Polym Sci A-Polym Chem*, 2015, 53: 405–412
19 Liu G, Liu M, Pu S, Fan C, Cui S. *Tetrahedron*, 2012, 68: 2267–2275
20 Gu PY, Lu CJ, Hu ZJ, Li NJ, Zhao T, Xu QF, Xu QH, Zhang JD, Lu JM. *J Mater Chem C*, 2013, 1: 2599
21 Lu C, Liu Q, Gu P, Chen D, Zhou F, Li H, Xu Q, Lu J. *Polym Chem*, 2014, 5: 2602
22 Zhang CY, He JH, Lu CJ, Gu QF, Wu LX, Liu Q, Li H, Xu QF, Lu JM. *Polymer*, 2015, 70: 343–350
23 Xia S, He J, Li H, Xu Q, Li N, Chen D, Lu J. *Sci China Chem*, 2016, 59: 692–698
24 Wang G, Miao S, Zhang Q, Liu H, Li H, Li N, Xu Q, Lu J, Wang L. *Chem Commun*, 2013, 49: 9470–9472
25 Gu QF, He JH, Chen DY, Dong HL, Li YY, Li H, Xu QF, Lu JM. *Adv Mater*, 2015, 27: 5968–5973
26 Gu PY, Zhou F, Gao J, Li G, Wang C, Xu QF, Zhang Q, Lu JM. *J Am Chem Soc*, 2013, 135: 14086–14089
27 Chu CW, Ouyang J, Tseng JH, Yang Y. *Adv Mater*, 2005, 17: 1440–1443
28 Liu CL, Chen WC. *Polym Chem*, 2011, 2: 2169